Integrated Analysis and Optimization of the Large Airborne Radome-Enclosed Antenna System

Chang Zhai, Xunwang Zhao, Zhongchao Lin, and Yu Zhang

Shaanxi Key Laboratory of Large Scale Electromagnetic Computing
Xidian University, Xi'an, Shaanxi 710071, China
xdzxw@126.com

Abstract ─ In order to realize integrally analysis and optimization of the large airborne radome-enclosed antenna system, a novel optimization strategy is proposed based on an overlapping domain decomposition method by using higher-order MoM and out-of-core solver (HO-OC-DDM), and combining with adaptive mutation particle swarm optimization (AMPSO). The introduction of parallel out-of-core solver and DDM can effectively break the random access memory (RAM) limit. This strategy can decompose difficult-to-solve global optimization problems into multi-domain optimization problems by using domain decomposition method. Finally, take airborne Yagi antenna system as an example, the numerical results show that the design of large airborne radome-enclosed antenna system based on the proposed strategy is convenient and effective.

Index Terms ─ AMPSO, HO-OC-DDM, integrated analysis and optimization, parallel algorithm.

I. INTRODUCTION

With the development of modern radar antenna technology, people no longer just design an antenna, but consider the antenna platform. The integrated design of the antenna is based on different environments and conditions. The aircraft is a sophisticated integrated platform, and the type and quantity of communication equipment on the aircraft are difficult to estimate. The traditional optimized design only considers the antenna or the radome-enclosed antenna. In more cases, the platform on which the antenna is installed needs to be considered together. However, whether the integrated analysis of the airborne antenna or the optimization of the radome-enclosed antenna is a difficult electromagnetic problem [1], and it is a challenging problem to consider the two together.

In order to solve these problems, many researchers have done a lot of research work. In early research, it mainly focused on the radome-enclosed antenna system. In the 1990s, FangHsu et al. of National Chiao Tung University analysed the radiation characteristics of a simple 2D radome-enclosed antenna system through formula calculation, and used simulated annealing to optimize the boresight error (BSE) by changing the radome thickness [2]. However, this method can only be used as a theoretical analysis and exploration and the convergence of the simulated annealing algorithm is relatively poor. In the early 21st century, Hidetoshi Chiba et al. adopted the Mutated PSO (MPSO) to optimize the thickness of the 2D radome-enclosed antenna system [3] and achieved better optimization results. Shortly after, Carlin et al. proposed a System-by-Design paradigm to design a 3D radome-enclosed antenna system. They analysed the electromagnetic problem by using the Electromagnetic Emulator, and optimized it by PSO [4]. This method successfully meets the requirements of practical project, but calculation accuracy of the Learning-by-Example regression strategy is poor. After that, Liu et al. used fast multipole method (FMM) to analyse the radome-enclosed antenna system and proposed a method of radial phase compensation to optimize the side-lobe level (SLL) [5]. There are also many researches on the radome-enclosed antenna [23,24], but the situation of radome-enclosed antenna with platform is not considered.

Recently, the optimization of platform-level system is still in the exploratory stage. For example, Wang et al. used a method of non-overlapping IE-DDM combined with PSO to optimize the antenna layout on a tank to reduce the overall RCS (Radar Cross Section) [6]. However, the antenna is a dipole antenna whose structure is simple and it is not working. Moreover, the PSO result is easy to trap in local optimum. For the integration optimization of the radome-enclosed antenna system platform, related research has not seen due to its large electrical size.

This paper is based on previous works, which are out-of-core Solver based DDM [7] and optimization of the radome-enclosed antenna arrays [8]. By combining of those, the integrated analysis and optimization of the large airborne radome-enclosed system is further achieved.

In the selection of numerical method, using higher-order MoM and out-of-core solver (HO-OC-MoM).

Submitted On: May 19, 2020
Accepted On: August 9, 2020

https://doi.org/10.47037/2020.ACES.J.351012

Firstly, HOMoM can ensure the accuracy of calculation and reduce memory consumption. The higher-order basis function [9,10] is used to approximate the current distribution, which produces less unknowns compared with the lower-order basis function. Secondly, the introduction of out-of-core solver can break the limitation of RAM [11].

In the optimization method selection and optimization model establishment, the current popular PSO is used. In order to avoid premature convergence, adaptive inertia weights and mutation operators [12, 13] are introduced to ensure the population diversity of the algorithm. Different from the traditional optimization model, we do not need to update and calculate the airborne radome-enclosed antenna system in the optimization iteration process. The strategy of multi-domain segmentation calculation and single-domain isolation optimization is used to avoid repeated calculation of the self-impendence inverse matrix in the same domain and be more convenient to modify the optimization model. This greatly improves the flexibility and convenience of the design.

The rest of this paper is organized as follows. In the Section II, the selection of higher order basis functions and the design of the out-of-core strategy are introduced. Meanwhile, the optimization strategy based on DDM used in this paper is introduced. In the Section III, a numerical example is given to illustrate the correctness and effectiveness of the algorithm. Finally, some conclusions are given in Section IV.

II. THEORETICAL ANALYSIS

A. Parallel out-of-core HOMoM

The geometric modeling of HOMoM is usually described by a bilinear quadrilateral, as shown in Fig. 1. For bilinear surfaces, the surface current density can be divided into *P* and *S*. In contrast to the lower-order basis functions, the higher-order basis functions introduce higher order terms to describe the surface current of the object and less unknowns are used to describe the object. Efficient approximation for the unknown currents is obtained by using higher-order basis functions:

$$\mathbf{F}_{ij}(p,s) = \frac{\boldsymbol{\alpha}_s}{\left|\boldsymbol{\alpha}_p \times \boldsymbol{\alpha}_s\right|} p^i s^j \qquad (1)$$
$$-\mathbf{1} \le p \le \mathbf{1}, -\mathbf{1} \le s \le \mathbf{1}.$$

Where $\boldsymbol{\alpha}_p$ and $\boldsymbol{\alpha}_s$ represent the tangential directions of the *P* and *S* parametric curves, respectively. The order of polynomial basis functions are *i* and *j*.

Taking the current as an example, it can be obtained:

$$\boldsymbol{J}_s(p,s) = \frac{\boldsymbol{\alpha}_s}{\left|\boldsymbol{\alpha}_p \times \boldsymbol{\alpha}_s\right|} \sum_{i=0}^{N_p} \left(\sum_{j=0}^{N_s} a_{ij} s^j \right) p^i . \qquad (2)$$

Taking the current continuity at the edge of the bilinear surface into account, the formula (3) can be obtained:

$$\boldsymbol{J}_s(p,s) = \sum_{i=0}^{N_p} \left[c_{i1} \boldsymbol{E}_{i1}(p,s) + c_{i2} \boldsymbol{E}_{i2}(p,s) + \sum_{j=2}^{N_s} a_{ij} \boldsymbol{P}_{ij}(p,s) \right], \qquad (3)$$
$$-1 \le p \le 1, -1 \le s \le 1$$

where c_{i1} and c_{i2} are:

$$c_{i1} = \sum_{j=0}^{N_s} a_{ij} (-1)^j \ , \ c_{i2} = \sum_{j=0}^{N_s} a_{ij} . \qquad (4)$$

If the bilinear surface is not connected with other patches, its surface current is only described by the basis function P_{ij}, which is called the patch basis function. Correspondingly, the basis function E_{ik} that is used to satisfy the current continuity on the common side of two or more bilinear surfaces is called the edge basis function. The use of edge basis function and patch basis function can well describe the current distribution on complex surfaces [14].

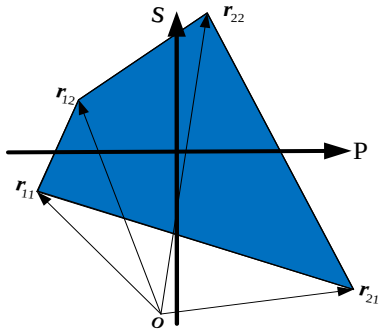

Fig. 1. Bilinear surface schematic.

When the problem is very complicated, HOMoM produces a very large complex density matrix. If the computer memory is unable to meet the storage needs, the hard disk is needed to store it. Generally speaking, the storage capacity of the hard disk is much larger than the memory capacity and easy to be expanded. Therefore, the out-of-core algorithm can not only greatly expand the computing scale of HOMoM, but also can extend the solution capabilities of DDM.

The out-of-core algorithm for HOMoM is divided into two parts: matrix filling and matrix solving. When the matrix is filled, the original matrix is divided into a series of sub-matrices suitable for the calculation in the core. Each sub-matrix is called a slab, which is written into the hard disk and repeats the process until the whole matrix is filled. The slab consists of M rows of the matrix, as shown in Fig. 2 and width of *i*th out-of-core slab is B_i, defined as:

$$M = \sum_{i=1}^{I_{slab}} B_i , \qquad (5)$$

where I_{slab} is a specific number of slab which is determined by the number of processes and the size of the matrix. Width of the last slab (i=I_{slab}) B_{last} is:

$$B_{last} = M - \sum_{i=1}^{I_{slab}-1} B_i . \tag{6}$$

When solving a matrix equation out of core, a part of the matrix is read into RAM and is performed LU factorization. The factorized matrix is written back to the hard disk. Then the next part is processed until the LU decomposition of the whole matrix is completed. This is the basic principle of the LU decomposition out of core. The detail of parallel out-of-core algorithm for HOMoM can be found in [7].

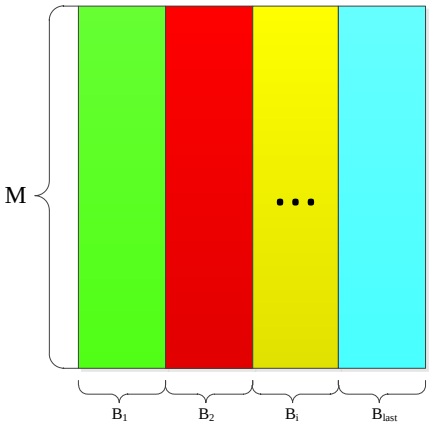

Fig. 2. Sub-matrix decomposition storage.

B. Optimization strategy based on DDM

The airborne radome-enclosed antenna system is a large-scale electromagnetic field problem. Nowadays, a lot of researches on domain decomposition are focused on scattering problems [22]. Radiation problems are still difficult to simulate and optimize. Therefore, according to the idea of the overlapping domain decomposition method [15, 16], the model is divided into several subdomains and each sub-domain is parallel solved independently. The coupling relationship and current continuity is considered by superimposing iteration. Then the optimal solution is finally optimized. As shown in Fig. 3, for a geometrically continuous object, the entire model can be properly divided into n sub-domains $\hat{\Omega}_i (i = 1,2,\ldots,n)$, and each subdomain contains its extended buffer $\hat{\Omega}_i = \Omega_i + \Omega_{Fi} + \Omega_{Bi}$, where Ω_{Fi} and Ω_{Bi} are forward buffer domain and backward buffer domain, respectively.

In this case, the matrix equation can be written as:

$$\begin{bmatrix} \mathbf{Z}_{11} & \mathbf{Z}_{12} & \cdots & \mathbf{Z}_{1j} & \cdots & \mathbf{Z}_{1n} \\ \mathbf{Z}_{21} & \mathbf{Z}_{22} & \cdots & \mathbf{Z}_{2j} & \cdots & \mathbf{Z}_{2n} \\ \vdots & \vdots & & \vdots & & \vdots \\ \mathbf{Z}_{i1} & \mathbf{Z}_{i2} & \cdots & \mathbf{Z}_{ij} & \cdots & \mathbf{Z}_{in} \\ \vdots & \vdots & & \vdots & & \vdots \\ \mathbf{Z}_{n1} & \mathbf{Z}_{n2} & \cdots & \mathbf{Z}_{nj} & \cdots & \mathbf{Z}_{nn} \end{bmatrix} \begin{bmatrix} \mathbf{I}_1 \\ \mathbf{I}_2 \\ \vdots \\ \mathbf{I}_i \\ \vdots \\ \mathbf{I}_n \end{bmatrix} = \begin{bmatrix} \mathbf{V}_1 \\ \mathbf{V}_2 \\ \vdots \\ \mathbf{V}_i \\ \vdots \\ \mathbf{V}_n \end{bmatrix}, \tag{7}$$

where Z_{ij} is the self-impedance matrix of the i-th domain Ω_i when i=j; Z_{ij} is the mutual-impedance matrix of domain Ω_j and domain Ω_i when $i \neq j$. I_i is the current coefficient vector of domain Ω_i, and V_i is the voltage vector of domain Ω_i.

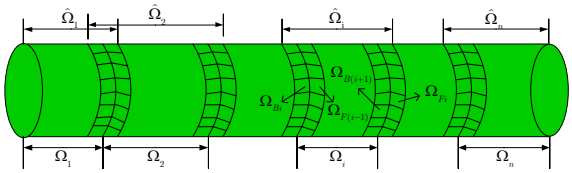

Fig. 3. DDM schematic of continuous object.

The Gauss Seidel iterative method is used to solve equation (7) and the convergence accuracy is set to δ. In order to ensure accuracy, HOMoM is used to solve the problems of each subdomain and the current continuity at the junction between the domains is ensured by iterative modifying the current of extended buffer. The domain $\hat{\Omega}_i$'s current coefficients can be expressed as:

$$\hat{\mathbf{I}}_i^{(k+1)} = -\hat{\mathbf{Z}}_{ii}^{-1} \sum_{j<i} \hat{\mathbf{Z}}_{ij} \mathbf{I}_j^{(k+1)} - \hat{\mathbf{Z}}_{ii}^{-1} \sum_{j>i} \hat{\mathbf{Z}}_{ij} \mathbf{I}_j^{(k)} + \hat{\mathbf{Z}}_{ii}^{-1} \hat{\mathbf{V}}_i , \tag{8}$$

where $\hat{\mathbf{I}}_i^{(k+1)}$ is the vector of current coefficients in domain $\hat{\Omega}_i$ to be solved during the k+1th iteration. $\mathbf{I}_j^{(k+1)}$ and $\mathbf{I}_j^{(k)}$ are the vector of current coefficients in extended buffer regions at the kth and k+1th iteration, respectively. $\hat{\mathbf{Z}}_{ii}$ and $\hat{\mathbf{Z}}_{ij}$ are the self-impedance matrix and mutual-impedance matrix, respectively.

If $\Delta\hat{\mathbf{V}}_i^{(k)} = \hat{\mathbf{Z}}_{ij}\mathbf{I}_j^{(k)}$, then formula (8) can be further written as:

$$\hat{\mathbf{Z}}_{ii}\hat{\mathbf{I}}_i^{(k+1)} = -\sum_{j<i} \Delta\hat{\mathbf{V}}_i^{(k+1)} - \sum_{j>i} \hat{\mathbf{Z}}_{ij} \Delta\hat{\mathbf{V}}_i^{(k)} + \hat{\mathbf{V}}_i . \tag{9}$$

The iteration is repeated until the residue $\varepsilon_i = \left\|\mathbf{I}_i^{(k+1)} - \mathbf{I}_i^{(k)}\right\| / \left\|\mathbf{I}_i^{(k+1)}\right\|$ satisfies $max\left(\varepsilon_1, \varepsilon_2, \cdots, \varepsilon_n\right) \leq \delta$ or the iteration number $k \geq k_{stop}$.

It is worth pointing out that there is no need to store the mutual-impedance matrix $\hat{\mathbf{Z}}_{ij}$, only the inner product of the field generated by electromagnetic current

$\mathbf{I}_j^{(k+1)}$ on region $\hat{\Omega}_i$ and the test function is used to calculate the coupling voltage, which is equivalent to directly calculating the product $\hat{\mathbf{Z}}_{ij} \cdot \mathbf{I}_j^{(k+1)} \left(j<i \right)$ or $\hat{\mathbf{Z}}_{ij} \cdot \mathbf{I}_j^{(k)} \left(j>i \right)$ in equation (9). In addition, the parallel out-of-core LU only needs to calculate $\hat{\mathbf{Z}}_{ii}^{-1}$ once. Then it can be stored in the hard disk and reused in the iteration between subdomains, which can greatly accelerate the calculation process. For more details about the DDM, please refer to our previous work [20,21].

The PSO algorithm is a popular intelligent evolutionary algorithm. However, it also has the disadvantages of premature convergence and easy to fall into local optimal solution. In view of these shortcomings, this paper introduces adaptive weights and variable particles to improve the convergence of algorithm. The adaptive inertia weight is used to dynamically adjust the search ability and the mutation is used to expand the diversity of the population [17,18,19].

The optimization strategy flow chart is shown in Fig. 4.

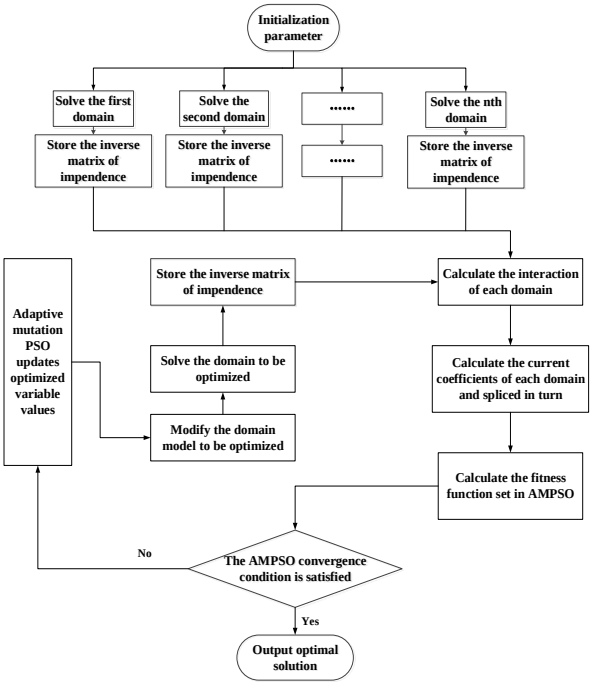

Fig. 4. Optimization strategy flow chart.

The optimized object is divided into n domains. Assuming that the first domain needed to be optimized and the other domains don't need to be optimized. The self-impendence inverse matrix of each domains is calculated and stored in hard disk during initialization. The coupling effect between each domain is calculated, and the current coefficient of each domain is calculated by Gauss Seidel iteration, and the overall object current coefficients is obtained by splicing in turn. According to the constraints set in AMPSO, the fitness function is calculated by using the overall object current coefficients. The fitness function is used to determine whether the optimization meets the conditions and needs to be terminated. If not, the optimization variables are updated through AMPSO to modify the domain model to be optimized. And the self-impendence inverse matrix of the domain to be optimized after the correction is calculated and stored in hard disk. Repeat the above operations until the termination conditions set by AMPSO are met. The basic idea of the optimization strategy is to use HO-OC-DDM to calculate the overall object current coefficients, so as to obtain the required fitness function of AMPSO. And then the domain to be optimized is modified through AMPSO. The two cooperate with each other to obtain the optimal solution. With this strategy, the electrically large-scale problem can be divided into several subproblems, and the calculation process of optimization fitness function can be accelerated by HO-OC-DDM, and achieve effective optimization.

III. INTEGRATED OPTIMIZATION AND ANALYSIS OF THE LARGE AIRBORNE YAGI ANTENNA ARRAY

The correctness of the parallel out-of-core HOMoM has been proved in the literatures [7, 20]. In the previous work, the author also carried out an optimized simulation investigating on the large radome-enclosed antenna system [8]. And did the comparison and verification of HO-OC-DDM with FEKO [7], which confirmed the effectiveness and reliability of the computing kernel. For the numerical example, the computations have been done on a workstation which consists of two eight-core 64 bit Intel Xeon E5-2620 2.0 GHz CPUs, 64GB RAM and 6TB disk.

In order to verify the algorithm, taking an aircraft platform loading an airborne radar as an example, the antenna is equipped with rotating radome to form the whole system. The radome-enclosed antenna model is shown in Fig. 5.

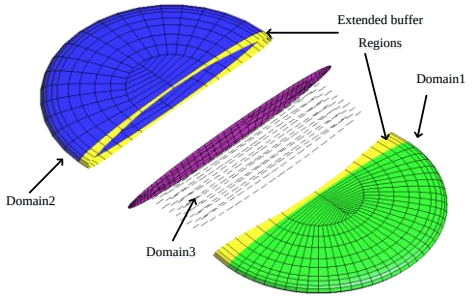

Fig. 5. The radome-enclosed antenna model.

The radome is a single medium with diameter being 8.4m, height 1m, thickness 24.8mm and ε_r=2.0. The antenna array consists of 38 Yagi antennas which are evenly arranged along the oval backplane. The working frequency is UHF. The airborne radome-enclosed antenna system consists of 4 domains. The number of unknowns of the system is 114,879.

In order to verify the accuracy of the HO-OC-DDM, the HOMoM (global solution) and the HO-OC-DDM are used to simulate the above-mentioned radome-enclosed antenna. The comparison result is shown in Fig. 6, the solid line and the dashed line represent the pattern curves of the HOMoM and the HO-OC-DDM, and the two curves basically overlap. The comparison of calculation resources between the HOMoM and the HO-OC-DDM is shown in Table 1. Compared with the HOMoM, the HO-OC-DDM takes less time and consumes less memory, which proves the efficiency of the HO-OC-DDM.

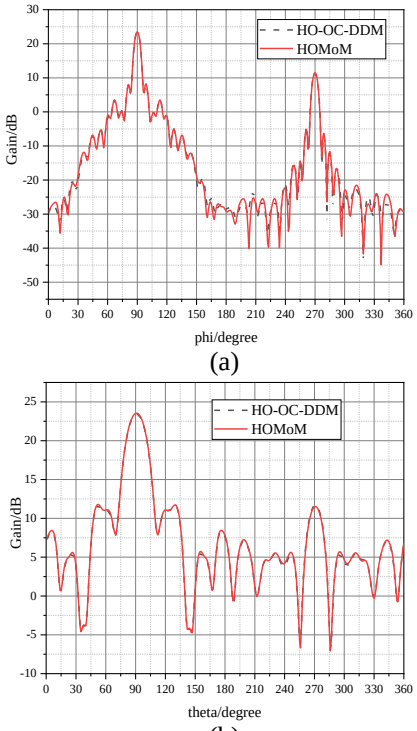

Fig. 6. Comparison results of HOMoM and HO-OC-DDM: (a) E-plane and (b) H-plane.

Table 1: Comparison results of HOMoM and HO-OC-DDM

Method	Unknowns		Storage/ GB	Core Number	Calculating Time/s
HOMoM	80,476		97	16	18642.256
HO-OC-DDM	Domain 1	44936	30	16	8503.215
	Domain 2	34728	14		
	Domain 3	2028	0.06		

Next, the antenna is mounted on the aircraft for integrated analysis and optimization. The whole platform of the aircraft is a metal structure, and the height of the radome is 0.815m. The model is shown in Fig. 7. The division is based on actual engineering experience and calculation difficulty. Table 4 shows the computing information of radiation characteristics analyzed by parallelized HO-OC-DDM and the simulated radiation pattern is shown in Fig. 8.

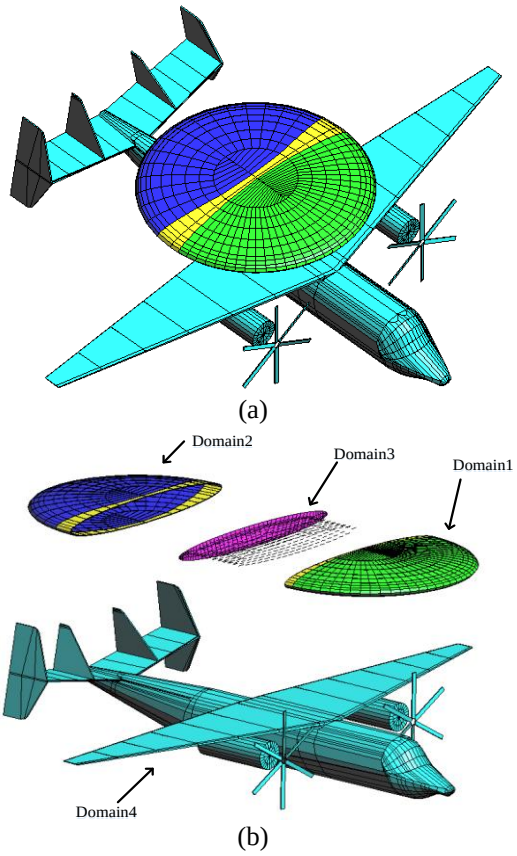

Fig. 7. Airborne radome-enclosed antenna system: (a) the entire system model, and (b) domain decomposition diagram.

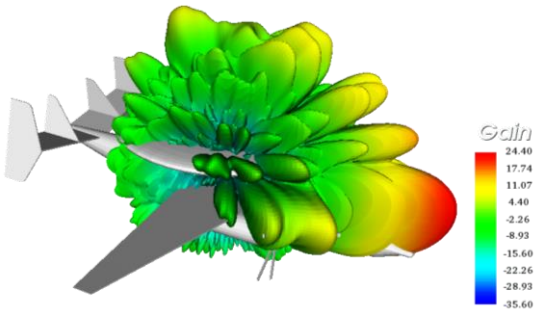

Fig. 8. 3D radiation pattern of airborne radome-enclosed antenna system before optimization.

It can be seen from the pattern, the aircraft cannot meet the performance requirements of high gain and low side lobe after the radome-enclosed antenna is installed. Thus the antenna needs to be optimized further. Here we choose to adjust the antenna structure and optimize the length of each element. The optimization goals come from the actual engineering experience. Such as keep the maximum gain greater than 24dB, the SLL at H-plane and E-plane are less than -15dB and the front-to-back ratio is greater than 15dB. The optimization model is as follows:

$$\begin{cases} \min\ fitness \\ s.t.\ G \geq 24dB,\quad FB \geq 15\text{dB} \\ SLL_H \leq -15\text{dB},\quad SLL_E \leq -15\text{dB} \\ l_{min} \leq l_{ij} \leq l_{max}\quad (1 \leq i \leq 10, 1 \leq j \leq 8) \end{cases}, \tag{10}$$

$$fitness = [\sum_{i=1}^{4} a_i max^2(-h_i, 0)]^{\frac{1}{2}} \tag{11}$$

$$h_1 = G - 14.5,\ h_2 = SLL_E + 15,\ h_3 = SLL_H + 15,\ h_4 = FB - 15$$

where G is the maximum gain of the antenna, SLL_H and SLL_E are the SLL of the E and H plane respectively, FB is the front-to-back ratio of the antenna pattern, l_{ij} is the length of the dipole and a_i is the weight of each constraint.

When the AMPSO is used to optimize of antenna, the population number chooses 40, the constraint weights are a_i={0.15,0.35,0.35,0.15}, both acceleration factor c_1 and c_2 take 2.0, the iterations number is 100 ,the adaptive inertia weight ρ_1 takes 0.9 and ρ_2 takes 0.3. After 100 iterations, the optimized radiation pattern is shown in Fig. 9. The optimized parameters and the variable results are shown in Table 2 and Table 3.

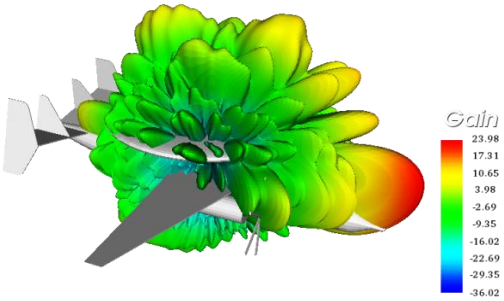

(a)

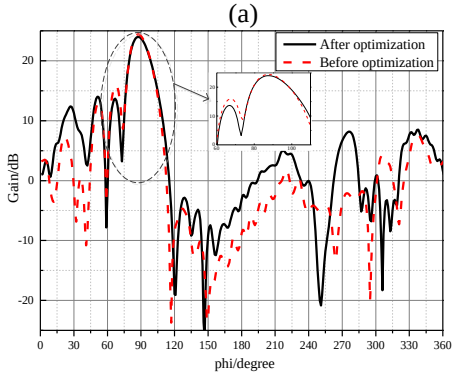

(b)

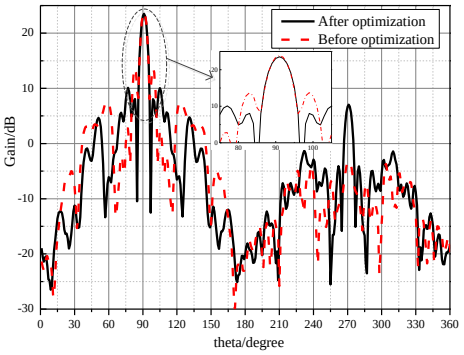

(c)

Fig. 9. Comparison of radiation patterns before and after optimization: (a) 3D, (b) E-plane, and (c) H-plane.

Table 2: Parameters of the system before and after optimization

Optimization Parameter	Before Optimization	After Optimization
Gain (dB)	24.4	23.98
E-plane SLL_E (dB)	-8.5	-10.3
H-plane SLL_H (dB)	-8.02	-15.88
F/B (dB)	26.4	17.3

Table 3: Optimization results of the system

Director Number	Optimization Results (m)	…	Director Number	Optimization Results (m)
$l_{1,1}$	0.14103	…	$l_{10,1}$	0.14153
$l_{1,2}$	0.14132	…	$l_{10,2}$	0.13098
$l_{1,3}$	0.1407	…	$l_{10,3}$	0.1137
$l_{1,4}$	0.1131	…	$l_{10,4}$	0.1139
$l_{1,5}$	0.14191	…	$l_{10,5}$	0.11334
$l_{1,6}$	0.11209	…	$l_{10,6}$	0.1081
$l_{1,7}$	0.11043	…	$l_{10,7}$	0.11309
$l_{1,8}$	0.1131	…	$l_{10,8}$	0.11315

Table 4: The system resource consumption

Unknowns		Storage (GB)	Number of CPU Cores	Initialization Time(s)	Single Iteration Time(s)
Domain 1	44936	30.09	16	12358.2	408.6
Domain 2	34728	17.9			
Domain 3	2028	0.06			
Domain 4	32656	15.8			

As can be seen from the above figures and tables, after the optimization, the gain of the airborne radome-enclosed antenna system is 23.98dB, which is slightly decreased, but it's basically close to the optimization target of 24dB. The E-plane and H-plane SLL have been reduced, the H-plane has met the optimization

goal and the E-plane has also been reduced by 1.8dB, with a certain optimization effect. Generally speaking, the main focus optimization goals are to meet the requirements, which can prove the effectiveness of the method.

In the initialization, all subdomains are calculated and spent 12,358s on a 16-core workstation. In the optimization process, only the optimized subdomain 3 is recalculated, which takes 409s per generation. In the calculation process, the out-of-core technology uses about 30GB RAM and 63.85GB hard disk. The entire optimization process takes about 15 hours. If HOMoM combining with PSO is used for optimization directly without DDM, one iteration calculation takes about 1600s using 192 cores. Calculating the same number of iterations for the same problem requires at least two months completing the optimization. The optimization efficiency is extremely low and the project is unacceptable. In contrast, DDM is not only more efficient and resource-saving for airborne radome-enclosed antenna integration optimization, but also more flexible and easy to operate.

V. CONCLUSION

This paper focuses on the analysis and optimization of the large airborne radome-enclosed antenna system. The analysis is based on high-precision full wave algorithm HOMoM. The solution is accelerated by combining parallel technology and out-of-core technology. The domain of interest is calculated separately by using DDM. Then the AMPSO algorithm is used to optimize this domain and the effects of the entire system are considered through the superposition of other domains. Numerical example shows that this method is suitable for the analysis and optimization of the airborne radome-enclosed antenna system, which provides a convenient and reliable research method for the integrated design of the antenna with platform.

ACKNOWLEDGMENT

This work was supported in part by the National Key Research and Development Program of China under Grant 2017YFB0202102, in part by the National Science Foundation of China under Grant 61901323, in part by the Colleges and Universities 20 Terms Foundation of Jinan City under Grant 2018GXRC015, in part by the Fundamental Research Funds for the Central Universities under Grant XJS190210.

REFERENCES

[1] B. Wang, M. He, J. Liu, C. Zhang, and H. Sun, "Fast and efficient analysis of radome-enclosed antennas in receiving mode by an iterative-based hybrid integral equation/modified surface integration method," in *IEEE Transactions on Antennas and Propagation*, vol. 65, no. 5, pp. 2436-2445, May 2017.

[2] F. Hsu, P. R. Chang, and K. K. Chan, "Optimization of two-dimensional radome boresight error performance using simulated annealing technique," in *IEEE Transactions on Antennas and Propagation*, vol. 41, no. 9, pp. 1195-1203, Sept. 1993.

[3] H. Chiba, Y. Inasawa, H. Miyashita, and Y. Konishi, "Optimal radome design with particle swarm optimization," *2008 IEEE Antennas and Propagation Society International Symposium*, San Diego, CA, pp. 1-4, 2008.

[4] M. Carlin, M. Salucci, L. Tenuti, P. Rocca, and A. Massa, "Efficient radome optimization through the system-by-design methodology," *2015 9th European Conference on Antennas and Propagation (EuCAP)*, Lisbon, pp. 1-3, 2015.

[5] L. Liu and Z. Nie, "Performance improvement of antenna array-radome system based on efficient compensation and optimization scheme," in *IEEE Antennas and Wireless Propagation Letters*, vol. 18, no. 5, pp. 866-870, May 2019.

[6] X. Wang, J. Hu, W. Zhu, M. Jiang, R. Zhao, and Z. Nie, "Antenna optimization based on non-conformal IE-DDM and PSO," *Proceedings of 2014 3rd Asia-Pacific Conference on Antennas and Propagation*, Harbin, pp. 1012-1015, 2014.

[7] Y. Li, X. Zhao, and H. Zhang. Out-of-core solver based DDM for solving large airborne array," *Applied Computational Electromagnetics Society Journal*, vol. 31, no. 5, pp. 509-515, 2016.

[8] C. Zhai, X. Zhao, Y. Wang, Y. Zhang, and M Tian, "PSO algorithm combined with parallel higher-order MoM to compensate the influence of radome on antennas," *Applied Computational Electromagnetics Society Journal*, vol. 32, no. 3, pp. 215-220, 2017.

[9] Z. Lin, Y. Chen, Y. Zhang, X. Zhao, and H. Zhang, "An efficient GPU-based out-of-core LU solver of parallel higher-order method of moments for solving airborne array problems," *International Journal of Antennas and Propagation*, pp. 1-10, Feb. 27, 2017.

[10] Y. Chen, S. Zuo, Y. Zhang, X. Zhao, and H. Zhang, "Large-scale parallel method of moments on CPU/MIC heterogeneous clusters," in *IEEE Transactions on Antennas and Propagation*, vol. 65, no. 7, pp. 3782-3787, July 2017.

[11] H. Midorikawa, K. Kitagawa, and H. Ohura, "Efficient swap protocol of remote memory paging for out-of-core multi-thread applications," *2017 IEEE International Conference on Cluster Computing (CLUSTER)*, Honolulu, HI, pp. 637-638, 2017.

[12] Z. Qin and Y. Liang, "A study on the particle swarm optimization with iAdaptive weight constrained layout optimization," *2016 8th International Conference on Intelligent Human-Machine Systems and Cybernetics (IHMSC)*, Hangzhou, pp. 283-287, 2016.

[13] J. A. Yacim and D. G. B. Boshoff, "Combining BP with PSO algorithms in weights optimisation and ANNs training for mass appraisal of properties," *International Journal of Housing Markets and Analysis, 2018 IJHMA*, 02-2017-0021, 2018.

[14] Y. Zhang, R. A. van de Geijn, M. C. Taylor, and T. K. Sarkar, "Parallel MoM using higher-order basis functions and PLAPACK in-core and out-of-core solvers for challenging EM simulations," in *IEEE Antennas and Propagation Magazine*, vol. 51, no. 5, pp. 42-60, Oct. 2009.

[15] R. Zhao, J. Hu, H. Zhao, M. Jiang, and Z. Nie, "FIE-PMCHWT-based domain decomposition method for solving electromagnetic scattering from complex dielectric/metallic composite objects," in *IEEE Antennas and Wireless Propagation Letters*, vol. 16, pp. 1293-1296, 2017.

[16] Z. Peng, R. Hiptmair, Y. Shao, and B. MacKie-Mason, "Domain decomposition preconditioning for surface integral equations in solving challenging electromagnetic scattering Problems," in *IEEE Transactions on Antennas and Propagation*, vol. 64, no. 1, pp. 210-223, Jan. 2016.

[17] K. Kiran Kumar, N. Venkata Ramana, and S. Kamakshaiah, "Global optimal solution for network reconfiguration problem using AMPSO algorithm," *2012 IEEE International Conference on Power System Technology (POWERCON)*, Auckland, pp. 1-7, 2012.

[18] H. Can, L. Juelong, and X. Jianchun, "A new model for structural damage assessment using adaptive mutation particle swarm optimization and support vector machine," *2018 Chinese Control And Decision Conference (CCDC)*, Shenyang, pp. 6711-6714, 2018.

[19] X. Li, X. Lyu, Y. Tong, S. Li, and D. Liu, "An object-based river extraction method via optimized transductive support vector machine for multi-spectral remote-sensing images," in *IEEE Access*, vol. 7, pp. 46165-46175, 2019.

[20] Y. Li, Y. Zhang, Z. Lin, Y. Wang, and X. Zhao, "Analysis of airborne array using parallel out-of-core higher-order DDM-MoM solver," *2015 IEEE International Symposium on Antennas and Propagation & USNC/URSI National Radio Science Meeting*, Vancouver, BC, pp. 1676-1677, 2015.

[21] Y. Liu, Q. Su, X. Zhao, Y. Zhang and C. Zhai, "Accurate analysis of JEM interference in airborne array characteristics using parallel HO-IE-DDM," *2018 Cross Strait Quad-Regional Radio Science and Wireless Technology Conference (CSQRWC)*, Xuzhou, pp. 1-3, 2018.

[22] K. Zhao, V. Rawat, and J. Lee, "A domain decomposition method for electromagnetic radiation and scattering analysis of multi-target problems," in *IEEE Transactions on Antennas and Propagation*, vol. 56, no. 8, pp. 2211-2221, Aug. 2008.

[23] J. W. You, S. R. Tan, X. Y. Zhou, W. M. Yu, and T. J. Cui, "A new method to analyze broadband antenna-radome interactions in time-domain," in *IEEE Transactions on Antennas and Propagation*, vol. 62, no. 1, pp. 334-344, Jan. 2014.

[24] H. Gao, Z. Peng, and X. Sheng, "A geometry-aware domain decomposition preconditioning for hybrid finite element-boundary integral method," in *IEEE Transactions on Antennas and Propagation*, vol. 65, no. 4, pp. 1875-1885, Apr. 2017.